Kinetic Model for Motion Compensation in Computed Tomography

Zhou Yu, Jean-Baptiste Thibault, Jiao Wang, Charles A. Bouman, and Ken D. Sauer

***Abstract*—Model based iterative reconstruction (MBIR) algorithms have recently been applied to computed tomography and demonstrated superior image quality. MBIR algorithms also have the potential to incorporate sophisticated models of data acquisition to address artifacts. In this paper, we introduce kinetic models to the MBIR framework, which allow voxel value to change as a function of time. Conventional reconstruction algorithms assume the voxels are constant over time. This assumptions is not true when patient motion is present, which, in turn, results in motion artifacts. Our approach to address this problem is to include such phenomena directly in the models of the cost function. We introduces a kinetic model for each voxel which is parameterized by a set of kinetic parameters. We then reconstruct the image by estimating these parameters in a MBIR framework. Results on phantom study and clinical data show that the proposed method can significantly reduce motion artifacts in the reconstruction.**

I. Introduction

Model based iterative reconstruction (MBIR) algorithms have recently been applied to computed tomography and demonstrated superior image quality performance [1], [2], [3]. These methods typically work by estimating the images that best fit the data based on the models of the system, the noise in the data, and the reconstructed image. To do this, the images are estimated by minimizing the following cost function,

$$\hat{x} = \arg\min_{x \geq 0} \left\{ \frac{1}{2}(y - Ax)^T D(y - Ax) + U(x) \right\} \qquad (1)$$

where x denotes the voxels in the image stored in a vector, and y denotes the vector form of the projection data. The models of the system are incorporated in equation (1). The forward model represented by the matrix A computes synthesized projection data based on the image. The accurate modeling of A is important for improving the spatial resolution and reducing geometric related artifacts. The noise model denoted by the diagonal matrix D models the signal to noise ratio of each measurement, and therefore it is important for noise reduction of the reconstruction. Last but not least, the image is regularized by the function $U(x)$ derived from a prior distribution on the image. With accurate modeling of geometry and noise, the MBIR algorithm can produce high resolution images with significantly reduced noise and artifacts. In order to further improve image quality, this algorithmic framework also provides the flexibility to incorporate more sophisticated physical models of the data acquisition process such as the spectrum of the X-ray [4], the gain fluctuation of the system [5], etc.

In this paper, we propose to incorporate a kinetic model into equation (1), which allows voxel values to change as a function of time. Conventional reconstruction algorithms typically assume that voxel values are constant during data acquisition. This assumption is violated when patient motion occurs or when using contrast agents in perfusion studies, for instance, which typically results in motion artifacts in the reconstructed images. Our approach to address this problem is to include such phenomena directly in the models of the cost function. We introduces a kinetic model for each voxel which is parameterized by a set of kinetic parameters. The objective is to reconstruct the image by estimating these parameters in a MBIR framework. To develop the kinetic parameter iterative reconstruction (KPIR) algorithm, we derive a cost function of the kinetic parameters. These parameters are then jointly estimated by minimizing the cost function. Based on the kinetic parameters, we can present a snapshot image at a desired point in time to freeze motion. We can also produce a 4D time sequence using the kinetic parameters to display the image volume as a function of time. The algorithm we propose is efficient in the sense that there is limited additional computational cost added compared to the conventional MBIR algorithm.

Kinetic modeling of voxel values and parametric reconstruction algorithms were originally developed for positron emission tomography (PET) and single photon emission computed tomography (SPECT). In dynamic PET and SPECT imaging, direct methods have been developed to estimate physiological parameters directly from the sinogram data [6], [7], [8], [9], [10]. The contribution of this paper is to introduce a kinetic reconstruction algorithm for transmission tomography problems, and apply it to motion artifact reduction. This paper is organized as following. In section II, we introduce our kinetic model, derive the cost function, and describes the numerical algorithm we used to minimize the cost function. Finally, in section III, we apply this algorithm to reconstruct both clinical and phantom data to evaluate the perform ace of the algorithm.

Zhou Yu and Jean-Baptiste Thibault are with GE Healthcare Technologies, 3000 N Grandview Bvd, W-1180, Waukesha, WI 53188. Email: zhou.yu@ge.com, jean-baptiste.thibault@med.ge.com

Jiao Wang and Ken Sauer are with the Department of Electrical Engineering, 275 Fitzpatrick, University of Notre Dame, IN 46556-5637, Email: jwang7@nd.edu, sauer@nd.edu

Charles Bouman is with the School of Electrical and Computer Engineering, Purdue University, West Lafayette, IN 47907-0501. Telephone: (765) 494-0340. Email: bouman@ecn.purdue.edu

II. Kinetic Parameter Reconstruction Algorithm

The key idea of our method is to model the voxel values as a function of time. We discretize the time window of the measurement into K intervals of width dt seconds. We use $y^{(k)}$ and $x^{(k)}$ to denote the vector of measurements and voxel values in the k^{th} time interval. A brute force method to perform temporal reconstruction would estimate one image for each time interval to obtain a sequence of K images over time. However, such method would increase the dimension of the problem by a factor K, and finding a suitable a numerical algorithm to obtain a stable solution would be challenging.

We reduce the dimension of the problem by introducing different kinetic models that parameterize possible voxel motion with a small number of parameters. Let φ denote a matrix of kinetic parameters, in which each row φ_s is a vector of kinetic parameters for voxel s. The kinetic model is a function that maps φ to the image at time t, that is,

$$x^{(k)} = F(\varphi, t_k) \tag{2}$$

where t_k is the sampling time of the k^{th} time interval.

Given the kinetic model, the estimate $\hat{\varphi}$ minimizes the following cost function of φ adapted from the MBIR framework.

$$\hat{\varphi} = \arg\min_{\varphi} \sum_{k=1}^{K} \{(y^{(k)} - A^{(k)} F(\varphi, t_k))^T D^{(k)} (y^{(k)} - A^{(k)} F(\varphi, t_k))\} + U(\varphi) \tag{3}$$

This cost function has two terms. The first term is a summation of a series of data mismatch penalty functions for each sampling time t_k, where $A^{(k)}$ represents the forward model and $D^{(k)}$ is a diagonal matrix that assigns weights to each measurement according to the statistical model. The second term, $U(\varphi)$, is a regularization function for the kinetic parameters that penalizes noise and outliers in the reconstruction.

Given this framework, developing a kinetic parameter reconstruction algorithm mainly consists of three tasks. First, we need to select a kinetic model $F(\cdot)$ appropriate to describe the realistic changes in object density over the length of the acquisition. Second, parameter estimation must be stabilized by choosing a prior model for the kinetic parameters leading to the explicit formulation of the regularization function $U(\varphi)$. Third, a numerical algorithm must be developed to solve the optimization problem in equation (4). In the following paragraphs, we propose various methods for each of these tasks.

A. Parameterized Kinetic Model

Similar to equation (2), we can write the value of voxel s as a function of time using the following relation

$$x_s(t) = F_s(\varphi_s, t) \tag{4}$$

where $F_s(\cdot)$ represents the kinetic model parameterized by a φ_s for each voxel s.

One possible choice is to represent voxel values as a linear combination of a set of basis functions. In this case, we can rewrite equation (4) in the following form

$$x_s(t) = \sum_{i=1}^{m} \varphi_{s,i} b_i(t) \tag{5}$$

where $b_i(t)$ is the i^{th} basis function. We sample the value of the voxels at time points t_k, $k = 1, 2, ...K$, and the sampled values are given by $x_{s,k} = x_s(t_k)$. We use $\vec{x}_s$ to denote the K by 1 vector of the values of voxel s sampled at different t_k, which is computed by

$$\vec{x}_s = M_s \varphi_s \tag{6}$$

where M is a K by 3 matrix formed by sampling the basis functions, that is, $[M_s]_{k,i} = b_i(t_k)$.

The choice of basis functions determines the space of the kinetic functions. In this paper, we use general polynomial basis functions defined as follows

$$b_i(t) = (t - T_s)^{i-1} \tag{7}$$

where $i = 1, 2, 3$, and T_s is the time when we would like to freeze the motion. In this case, the parameter φ_1 is the image at time T_s. Other general basis function such as cosine and spline basis functions can also be used.

B. Prior Model

Estimating multiple parameters per voxel from the same amount of acquired data as available for conventional MBIR reconstruction can be unstable without the use of regularization. To stabilize this process, we assume the kinetic parameters follow certain prior models. We use $U(\varphi)$ to denote the regularization function of the kinetic parameters derived from the prior model.

Using the polynomial basis function described in equation (7), the parameter $\varphi_{s,1}$ is the final image displayed to the user, and therefore we use the same spatial image regularization approach as in conventional MBIR for $\varphi_{s,1}$. The regularization function of $\varphi_{s,1}$ can then be written generally as

$$U_1(\varphi_1) = \sum_{\{s,q\} \in \partial s} b_{sq} \rho(\varphi_{s,1} - \varphi_{q,1}) \tag{8}$$

where ∂s denotes the neighborhood of voxel s, b_{sq} are directional coefficients, and $\rho(\cdot)$ is the potential function that penalizes large variations in the parameters.

We also apply additional prior models to regularize the temporal changes in the voxel values. A simple prior model would assume the kinetic parameters are independent of each other. In this paper, we use L_2 norm regularization for the kinetic parameters given as follows

$$U_i(\varphi_i) = \frac{1}{\sigma_i^2} \sum_s \varphi_{s,i}^2 \tag{9}$$

where $U_i(\cdot)$ is the regularization function for the i^{th} component of the kinetic parameters, σ_i^2 adjusts the regularization strength. This particular prior model assumes that motion with large magnitude is less likely to happen, and therefore penalizes large values in the kinetic parameters more than small values.

C. Parametric Iterative Coordinate Descent Algorithm (PICD)

We use the parametric iterative coordinate descent (PICD) [6] algorithm to solve the optimization problem in equation (4). The key idea of the PICD algorithm is to update one voxel at a time, while all the kinetic parameters of the voxel are updated simultaneously. When voxel s is updated, the kinetic parameters of all other voxels are fixed in the cost function, and we can then minimize the global cost function over φ_s only.

For each voxel update, we first compute the first and second derivative of the data mismatch term in the cost function with respect to the current voxel s. The first derivative, denoted by θ_1, is a K by 1 vector, and the second derivative, θ_2, is a K by K diagonal matrix. θ_1 and θ_2 are computed directly from the error sinogram data by

$$[\theta_1]_k \leftarrow \sum_i d_{i,k} a_{i,s,k} e_{i,k} \tag{10}$$

$$[\theta_2]_{kk} \leftarrow \sum_i d_{i,k} a_{i,s,k}^2, \tag{11}$$

where $a_{i,s,k} = [A^{(k)}]_{i,s}$, and $e_{i,k}$ and $d_{i,k}$ respectively denote the elements in the error sinogram and the corresponding statistical weight.

Let $\hat{\varphi}_s$ denote the values of the parameter after the update, and $\tilde{\varphi}_s$ denote the values before the update. Let $\Delta\varphi_s = \hat{\varphi}_s - \tilde{\varphi}_s$. We can then write the optimization problem for voxel s as

$$\Delta\varphi_s \leftarrow \arg\min_{\Delta\varphi_s} \left\{ \theta_1^T M_s \Delta\varphi_s + \frac{1}{2} \Delta\varphi_s^T M_s^T \theta_2 M_s \Delta\varphi_s + U(\varphi) \right\} \tag{12}$$

With $Q_1 = \theta_1^T M_s - \tilde{\varphi}_s^T M_s^T \theta_2 M_s$ and $Q_2 = M_s^T \theta_2 M_s$, then it is equivalent to solve

$$\hat{\varphi}_s \leftarrow \arg\min_{\varphi_s} \left\{ Q_1 \varphi_s + \frac{1}{2} \varphi_s^T Q_2 \varphi_s + U(\varphi) \right\}. \tag{13}$$

After the update of φ_s using equation (13), the change in the parameters is forward projected into the sinogram domain. The sinogram update is done in two steps. First, we compute the change in the vector $\vec{x}_s$ using the following relation.

$$\Delta\vec{x}_s = M_s \Delta\varphi_s \tag{14}$$

Next, for each sample time t_k, we project the change in voxel value $\Delta x_{s,k}$ onto the error sinogram

$$e_{*,k} \leftarrow e_{*,k} + A_{*,s}^{(k)} \Delta x_{s,k} \tag{15}$$

III. Experimental Results

We implemented the KPIR algorithm using the kinetic models described in equation (7), and the prior model given by equations (8) and (9). We used PICD as the numerical algorithm to solve the optimization problem.

This algorithm was applied to both a motion phantom and clinical reconstructions. Figure 1 compares the reconstructions on the Quasar motion phantom. This motion phantom has a dense insert with an air chamber in the center moving at the programmable speed of 40 beats per minute in this particular scan. Figure 1 (a) shows the reconstruction without motion correction: significant motion artifacts appear as shadings in a large area around the air pocket. After applying KPIR, the reconstruction in (b) shows that the motion artifacts are significantly reduced and localized near the air bubble. The artifact reduction can also be verified by comparing the converged residual error sinograms. Figure 1 (c) and (d) shows the error sinogram corresponds to the reconstructions in (a) and (b). The residual error sinogram computed as $Ax - y$ illustrates the inconsistency between the image and the measurements. By comparison with the error sinogram without motion correction shown in (c), it is clear that the large errors are significantly reduced by the KPIR algorithm in (d).

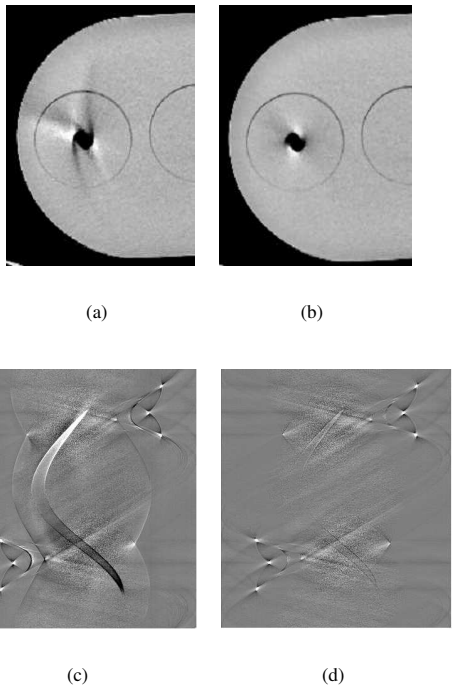

(a) (b) (c) (d)

Fig. 1. Comparison of algorithms on the Quasar motion phantom. The conventional reconstruction in (a) shows motion artifacts appearing as shadings near the moving air chamber. These artifacts are significantly reduced by KPIR as shown in (b). In (c) and (d), we compare the converged residual error sinograms computed by forward projecting the image and subtracting the data for both reconstructions: the conventional reconstruction in (c), and the KPIR in (d). The large remaining inconsistency in (c) cannot be explained by the conventional model as it is caused by the phantom motion. The error is significantly reduced in (d).

The proposed algorithm also have the flexibility to reconstruct images with different choices of T_s. We typically choose $T_s = T_{s,0}$, where $T_{s,0}$ is the center of the temporal window during which the voxel is measured by X-ray. Figure 2 shows the reconstruction of the motion phantom with $T_s = T_{s,0} - 0.25$, $T_{s,0}$, and $T_s = T_{s,0} + 0.25$ second, separately. Although there are some remaining motion artifacts, we can clearly see how the air bubble enters this slice, and its diameter grows as a function of time. In clinical reconstructions, this feature would allow us to choose T_s to reconstruct images at different phases.

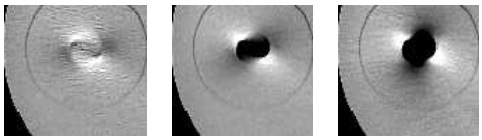

(a) (b) (c)

Fig. 2. Comparison of the images reconstruct with different T_s. The image in (b) is reconstructed using KPIR with $T_s = T_{s,0}$, the center of the temporal window of measurement. The image in (a) and (c) are reconstruct with $T_s = T_{s,0} - 0.25$ sec and $T_s = T_{s,0} + 0.25$ sec respectively. Although there are some remaining motion artifacts, we can clearly see how the air bubble enters this slice, and its diameter grows as a function of time.

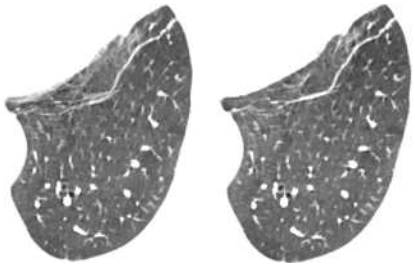

(a) (b)

Fig. 3. Comparison of the algorithms on clinical study. The conventional reconstruction in (a) shows a ghosting artifact near the heart wall and blurred vessels due to cardiac and respiratory motion. These artifacts are significantly reduced by KPIR as shown in (b).

Figure 3 compares the reconstruction using various algorithms on a clinical case. The images are zoomed into the chest region to focus on respiratory motion. Figure 3 (a) shows the conventional reconstruction without kinetic modeling. Due to cardiac and respiratory motion, the heart wall boundary shows a ghosting artifact and one of the vessels in the lung is significantly blurred. In this case, the KPIR algorithm appears effective in reducing both artifacts, as illustrated in (b).

Figure 4 compares the convergence speed between KPIR and MBIR algorithm. We run both algorithms for 20 iterations to produce a set of reference images. Then we compute the root mean square error (RMSE) for both algorithm during the reconstructions. In (a), the computational cost is measured by number of updates in the unit of iteration. The plot shows that KPIR and MBIR has very similar per iteration convergence speed. In (b), the computational cost is measured by the wall clock time normalized by 1 iteration time of MBIR. In this plot, KPIR is slightly slower since the computational cost per voxel update of KPIR is about 15% higher than MBIR on average.

IV. Conclusion

In this paper, we present a method of model based motion artifact reduction by introducing kinetic models to the MBIR framework. The phantom and clinical results show that the proposed algorithm can effectively reduce motion artifacts. The kinetic model we use in this paper is relatively simple. In the future, we can potentially improve this method by introducing more sophisticated kinetic model or prior model of the kinetic parameters.

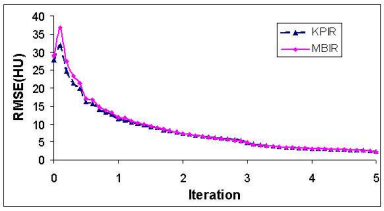

(a)

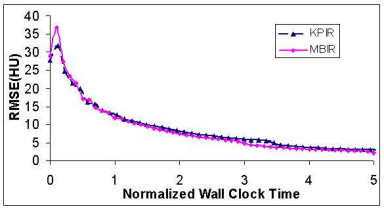

(b)

Fig. 4. This figure compares the convergence speed between KPIR and the MBIR. The image quality is measured by the RMSE of the image, and the computational cost is measured by the iteration in (a), and by the wall clock time normalized by the time of 1 iteration of MBIR in (b).

References

[1] J.-B. Thibault, K. D. Sauer, C. A. Bouman, and J. Hsieh, "A three-dimensional statistical approach to improved image quality for multi-slice helical CT," *Med. Phys.* **34**(11), pp. 4526–4544, 2007.

[2] A.Ziegler, Th.Köhler, and R.Proksa, "Noise and resolution in images reconstructed with FBP and OSC algorithms for CT," *Med. Phys.* **34**(2), pp. 585–598, 2007.

[3] Z. Yu, J.-B. Thibault, C. Bouman, K. Sauer, and J. Hsieh, "Fast model-based X-ray CT reconstruction using spatially nonhomogeneous icd optimization," *IEEE Trans. on Image Processing* **20**(1), pp. 161–175, 2011.

[4] I. Elbakri and J. A. Fessler, "Statistical image reconstruction for polyenergetic X-ray computed tomography," *IEEE Trans. on Medical Imaging* **21**(2), pp. 89–99, 2002.

[5] J.-B. Thibault, Z. Yu, K. Sauer, C. Bouman, and J. Hsieh, "Correction of gain fluctuations in tomographic iterative reconstruction," in *Proc. Intl. Conf. on Fully 3D Reconstruction in Radiology and Nuclear Medicine*, (Lindau, Germany), July 9-13 2007.

[6] M. Kamasak, C.A.Bouman, E. Morris, and K. Sauer, "Direct reconstruction of kinetic parameter images from dynamic pet data," *IEEE Trans. on Medical Imaging* **24**(5), pp. 636–650, 2005.

[7] S. Meikle, J. Matthews, V. Cunningham, D. Bailey, L. Livieratos, T.Jones, and P. Price, "Parametric image reconstrctuion using spectral analysis of pet projection data," *Phys. Med. Biol* **43**, pp. 651–666, 1998.

[8] J. Matthews, D. Bailey, P. Price, and V. Cunningham, "The direc calculation of parametric images from dynamic pet data using maximum-likelihood iterative reconstruction," *Phys. Med. Biol* **42**, pp. 1155–1173, 1997.

[9] E. Gravier, Y. Yang, and M. Jin, "Tomographic reconstruction of dynamic cardiac image sequences," *IEEE Trans. on Image Processing* **16**(4), pp. 932–942, 2007.

[10] B. Reutter, G. Gullberg, R. Boutchko, K. Balakrishnan, E. Botvinick, and R. Huesman, "Fully 4-d dynamic cardiac SPECT image reconstruction using spatiotemporal b-spline voxelization," in *Nuclear Science Symposium Conference Record, 2007. NSS '07. IEEE*, **6**, pp. 4217 –4221, Nov. 3 2007.